

Modeling of the perpendicular polarizer-planar free layer spin torque oscillator: Micromagnetic simulations

I. Firastrau,^{1,2,3} D. Guskova,¹ D. Houssameddine,¹ U. Ebels,¹ M.-C. Cyrille,² B. Delaet,² B. Dieny,¹ O. Redon,² J.-Ch. Toussaint,^{4,5} and L. D. Buda-Prejbeanu^{1,5}

¹*Spintec, URA 2512, CEA/INAC-CNRS, CEA-Grenoble, 17 Rue des Martyrs, 38054 Grenoble, France*

²*CEA-LETI, Minatec, DRT/LETI/DIHS, 17 Rue des Martyrs, 38054 Grenoble, France*

³*Transilvania University of Brasov, 29 Bld. Eroilor, R-500036 Brasov, Romania*

⁴*Institut Néel, CNRS, 25 Rue des Martyrs, 38042 Grenoble, France*

⁵*Institut Polytechnique de Grenoble, 46 Avenue Félix Viallet, 38031 Grenoble, France*

(Received 26 October 2007; published 28 July 2008)

Micromagnetic simulations are presented to describe the magnetization dynamics of a spin torque oscillator that combines an out-of-plane magnetized polarizer with an in-plane magnetized free layer. This oscillator configuration provides the possibility to excite large-angle out-of-plane steady-state oscillations of the free layer magnetization above a threshold current and in zero external field. While in a macrospin approximation, the frequency of these oscillations increases monotonously with increasing current density, the full micromagnetic simulations reveal two branches for the frequency vs current dependency: a first branch at lower current density with increasing frequency for increasing current, and a second branch at larger current density where the frequency decreases. This behavior has also been observed in our experiments and can be explained by the formation of a nonhomogenous magnetization configuration that tends to minimize the demagnetization field energy. However, the frequencies observed in the experiments are lower than in the simulations. We therefore investigate the influence of the Ampère field, the damping constant, the static dipolar interaction field from adjacent layers, and the sample shape on the magnetization configuration and the frequency vs current dependence.

DOI: [10.1103/PhysRevB.78.024437](https://doi.org/10.1103/PhysRevB.78.024437)

PACS number(s): 78.20.Bh, 75.75.+a, 72.25.Ba

I. INTRODUCTION

The ability to manipulate the magnetization state of a small magnetic element using a spin polarized current has opened the way to a new class of devices, such as the spin torque nano-oscillator¹ (STNO). A spin torque nano-oscillator is a magnetoresistive device that contains two ferromagnetic layers separated by a nonmagnetic interlayer. When an electric current passes perpendicularly to the plane of the device, the conduction electrons are spin polarized in the direction of the magnetization of a first layer (polarizing layer). At sufficiently high-current density, periodical oscillations of the magnetization can be generated in the second layer (free layer) via the spin transfer torque effect.^{2,3} These oscillations were first observed for in-plane magnetized spin valves,^{4–8} only in the presence of an external magnetic field, applied parallel, or perpendicular to the plane of the film. In contrast to this, theoretical studies have shown that large-angle out-of-plane (OPP) steady-state precessions of the free layer magnetization can be excited above the threshold current without any external field when using a geometry for which the polarizer (Pol) is oriented out of plane, while the free layer (FL) maintains an in-plane magnetization^{1,9–14} [see Fig. 1(a)]. Recently this concept has been verified experimentally.¹⁵ However, from the experiment it has been observed that the frequency vs current dependence deviates from macrospin predictions.^{1,9,13,14} It is therefore important to analyze the dynamics of the micromagnetic configuration of this “perpendicular” spin torque nano-oscillator using three-dimensional (3D) micromagnetic simulations.

The first part of this paper describes briefly the micromagnetic model (Sec. II). We then introduce in Sec. III the

current-field state diagram in the macrospin approximation, which summarizes the different possible magnetic states for the perpendicular polarizer configuration shown in Fig. 1(a). These states are modified when considering the full micromagnetic configuration (Sec. IV). Finally, we indicate how the Ampère field (Sec. V), the damping parameter (Sec. VI), the static dipolar interaction fields from adjacent layers (Sec. VII), as well as an elliptical sample shape (Sec. VIII) influence the dynamic micromagnetic configuration and the frequencies of the OPP steady-state oscillations.

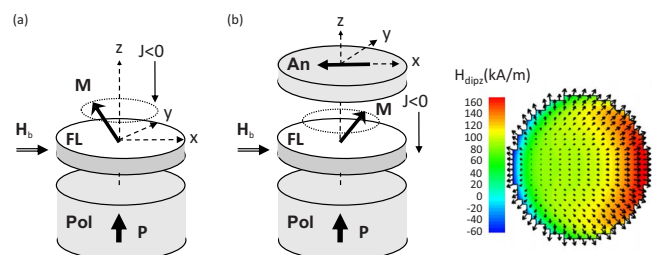


FIG. 1. (Color online) Schematics of the perpendicular polarizer configuration considering (a) the Pol and FL only and (b) the complete structure as in experiment with Pol, FL, and An. To the right is the distribution of the total static dipolar interaction field at the position of the free layer emanating from the perpendicular polarizer and the planar analyzing layer. The arrows correspond to the in-plane field component and the color code represents the out-of-plane field component. The values of the dipolar field are stated in kA/m. Here 160 kA/m correspond to 2 kOe.

II. MICROMAGNETIC MODEL

The dynamics of the magnetization vector \mathbf{M} is generally described by the Landau-Lifshitz-Gilbert (LLG) equation,¹⁶

$$\left(\frac{\partial \mathbf{M}}{\partial t}\right) = -\gamma \mathbf{M} \times \mathbf{H}_{\text{eff}} + \frac{\alpha}{M_s} \left(\mathbf{M} \times \frac{\partial \mathbf{M}}{\partial t}\right), \quad (1)$$

with γ as the gyromagnetic factor and α as the Gilbert damping parameter. \mathbf{H}_{eff} represents the effective field¹⁷ that accounts for the magnetic anisotropy \mathbf{H}_u , the externally applied fields \mathbf{H}_b , the exchange field \mathbf{H}_{ex} , and the demagnetizing field \mathbf{H}_D ,

$$\mathbf{H}_{\text{eff}} = \mathbf{H}_u + \mathbf{H}_b + \mathbf{H}_{\text{ex}} + \mathbf{H}_D. \quad (2)$$

Since the spin polarized current generates a torque on the magnetization, Slonczewski² proposed to modify the LLG Eq. (1) by adding a new term,

$$\left(\frac{\partial \mathbf{M}}{\partial t}\right)_{\text{ST}} = -\gamma a_J [\mathbf{M} \times (\mathbf{M} \times \mathbf{P})]. \quad (3)$$

Here \mathbf{P} is the spin-polarization vector, which is parallel to the polarizer magnetization (see Fig. 1) and a_J represents the amplitude of the spin torque term proportional to the injected current density J flowing through the system. a_J is expressed as

$$a_J = \frac{\hbar}{2e\mu_0 M_s t} g(\eta, \theta_p) J, \quad (4)$$

with \hbar as Planck's constant, e as the negative electron charge, and μ_0 as the magnetic permittivity in vacuum. M_s is the saturation magnetization of the free layer and t its thickness. Finally, the factor $g(\eta, \theta_p)$ is the angular-dependent spin-polarization efficiency,² which is a function of the spin polarization η and the angle θ_p between the magnetization \mathbf{M} and the spin-polarization vector \mathbf{P} . Here we have used the form given in Eq. (5) from Ref. 2,

$$g(\eta, \theta_p) = \left[-4 + \frac{1}{4} \frac{(1 + \eta)^3}{\eta^{3/2}} \left(3 + \mathbf{P} \cdot \frac{\mathbf{M}}{M_s} \right) \right]^{-1}. \quad (5)$$

To solve these equations a dedicated micromagnetic solver has been developed (ST-GLFFT) based on a finite differences approximation.¹⁸ The mesh cell size used in the simulations is $2 \times 2 \times 3.5$ nm³ and for the injected current step we considered a rise time of 2 ns. The demagnetizing field is evaluated by fast Fourier transform techniques and the integration scheme implicitly conserves the magnetization amplitude. The effects of thermal fluctuations are not taken into account in this study.

The spin torque nano-oscillator investigated here is a circular-shaped nanopillar of 60 nm in diameter. The bias field H_b is applied parallel to the $+x$ direction. The configuration mimics to some extent the STNO studied in the experiments of Ref. 15. Here two different cases are considered: (i) one consisting of only the polarizer and the free layer as defined in Fig. 1(a) and (ii) one having an analyzing (An) layer above the free layer, as shown in Fig. 1(b). In the experiments this analyzing layer is required in order to produce a measurable magnetoresistive signal proportional to

TABLE I. Material parameters used in the simulation for the Pol, FL, and An. A_{ex} is the exchange energy and H_u the uniaxial anisotropy field (parallel to the x direction) that has been considered only for circular disks. The values for M_s and the layer thicknesses correspond to the sample structure investigated in Ref 13. Similarly α and η are values that were used in Refs. 13 and 14.

	M_s in kA/m (emu/cm ³)	t (nm)	α	η	A_{ex} (J/m)	H_u in A/m (Oe)
Pol	1015 (1015)	6				
FL	886 (886)	3.5	0.01	0.3	2×10^{11}	1200 (15)
An	1400 (1400)	3				

the oscillating free layer magnetization component parallel to the analyzing layer. The inhomogeneous static dipolar interaction fields from the analyzer and the polarizer magnetization are shown in Fig. 1(b) (right) and can modify the dynamic response of the free layer magnetization (see Sec. VII).

The parameters used in the simulations are summarized in Table I. In our model we assumed that only the free layer magnetization can evolve under the action of the effective field and of the perpendicularly injected current ($\parallel Oz$), while the magnetization of the polarizer ($\parallel +Oz$) and of the analyzer ($\parallel -Ox$) are fixed. Moreover, we have taken into account only a spin torque due to perpendicularly polarized electrons, so $\mathbf{P} = (0, 0, 1)$. Simulations considering also contributions to the spin torque from in-plane-polarized electrons due to the presence of the analyzer do not modify substantially the presented results.¹⁹

The current flowing through the pillar generates itself a magnetic field, which is accounted for in the effective field including an additional term called Ampère field \mathbf{H}_{Amp} . The Ampère field is numerically evaluated using the hypothesis of a homogeneous current density in the pillar and by supposing that the electrodes are situated at 87.5 nm distance from the free layer. For all calculations, except some of Sec. VIII, the initial state of the free layer magnetization is in-plane and parallel to the $+Ox$ direction.

III. MACROSPIN DIAGRAM AND FREQUENCY

First, we summarize macrospin simulations that show the current-field state diagram, defining different static and dynamic states of the FL magnetization.^{13,14} In Sec. IV, these results are compared with micromagnetic simulations for the case of zero applied bias field. One of the interesting features of the spin transfer torque is that it can induce magnetization states that cannot be obtained by using external magnetic fields;^{20–22} namely, it can either generate large-angle steady-state oscillations of the magnetization or it can rotate the magnetization into static positions, which are not energy minima. For the “perpendicular polarizer-planar free layer” configuration shown in Fig. 1(a), these states are summarized in Fig. 2(a) in a current-field (J - H_b) state diagram as calculated in the macrospin approach.^{11,13–15}

There are three possible states upon increasing the *ampli-*

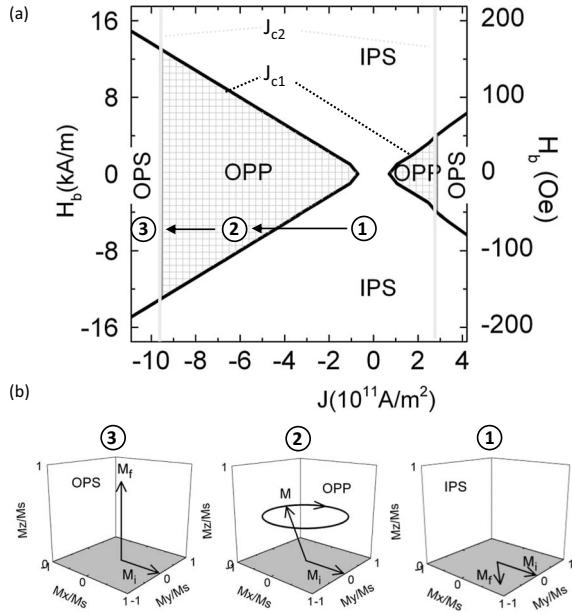


FIG. 2. (a) Macrospin current-field state diagram, revealing three different states: the in-plane stable state IPS, the out-of-plane stable state OPS, and the out-of-plane precession state OPP. J_{c1} is the critical line separating IPS and OPP. J_{c2} is the critical line separating OPP and OPS. (b) The IPS, OPP, and OPS states are shown in a 3D plot for the case of negative current density. M_i corresponds to the initial orientation of the magnetization at the start of the simulation and M_f corresponds to the final orientation of the magnetization.

tude of the current density that are illustrated in Fig. 2(b): a static in-plane stable (IPS) state for $0 < |J| < |J_{c1}|$, a dynamic OPP state for $|J_{c1}| < |J| < |J_{c2}|$, and a static out-of-plane stable (OPS) state for $|J| > |J_{c2}|$. In the IPS state the spin torque is balanced by the precession torque (determined by H_u and H_b) leading to an in-plane rotation of the FL magnetization.^{13–15} Similarly, in the OPS state, the magnetization rotates out-of-plane and stabilizes close to the out-of-plane energy maximum. We note that in the OPS state the magnetization rotates into the positive z direction (parallel to \mathbf{P}) for negative current $J < 0$ and into the negative z -direction (antiparallel to \mathbf{P}) for positive current $J > 0$.

In the following part we focus only on the OPP state, which is stabilized when the spin torque balances the damping torque averaged over one precession period such that the magnetization continuously oscillates around the out-of-plane energy maximum.^{15,21} For increasing current amplitude, the absolute value of the critical current-density amplitude $|J_{c1}|$ required to produce OPP oscillations depends on the applied bias field^{13–15} leading to the triangular shape of the OPP regions of Fig. 2(a). As can be seen, the state diagram is asymmetric with respect to the current direction, with a larger region of the OPP state for negative current than for positive current.^{13,14} This asymmetry is also reflected in the frequency versus current dispersion shown in Fig. 3(a) (full line) for which the slope is steeper in positive current than in negative current.

The asymmetry is due to the angular dependence of the spin-polarization efficiency $g(\eta, \theta_p)$ Eq. (5) yielding a stron-

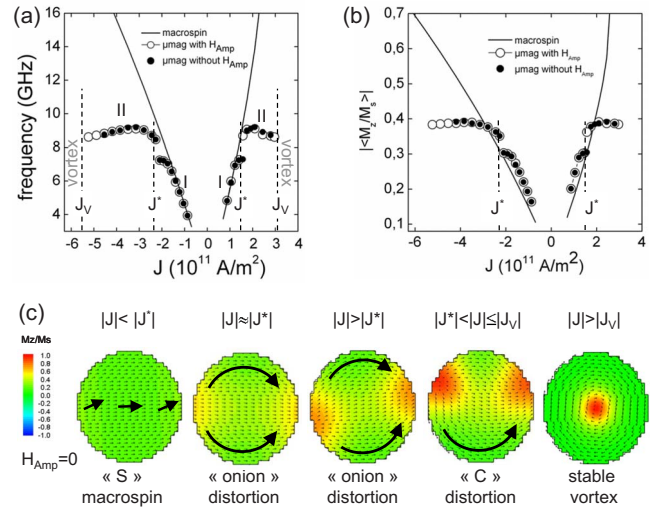


FIG. 3. (Color online) (a) Frequency f versus current-density amplitude J for a circular disk of 60 nm diameter and for the configuration shown in Fig. 1(a), as obtained from macrospin simulations (full line) as well as from micromagnetic simulations, without Ampère field (full dots) and with Ampère field H_{Amp} (open dots). The current density J^* denotes the transition from branch I to branch II and J_V the transition from branch II to the static vortex state (the vertical dashed line indicates the transition in the case of nonzero Ampère field). (b) Normalized average absolute value of the out-of-plane magnetization component $\langle M_z/M_s \rangle$ as a function of current-density amplitude for the macrospin (full line) and micromagnetic simulations (full dots, open dots). (c) Top view of the magnetization configuration of the free layer for different negative values of the current density (no Ampère field) from left to right at $J = -1.1 \cdot 10^{11} \text{ A/m}^2$ corresponding to branch I, $J = -2.3 \cdot 10^{11} \text{ A/m}^2$ corresponding to the transition at J^* , $J = -3.2 \cdot 10^{11} \text{ A/m}^2$ corresponding to branch II, and $J = -4.6 \cdot 10^{11} \text{ A/m}^2$ before the transition to the vortex state. The arrows indicate the in-plane magnetization component and the color code the out-of-plane magnetization component.

ger contribution when \mathbf{M} and \mathbf{P} are antiparallel ($J > 0$) than for the case when \mathbf{M} and \mathbf{P} are parallel ($J < 0$)². As explained in Ref. 14, $g(\eta, \theta_p)$ can be considered as a scaling factor for the current axis, which means that, for example, for a larger $g(\eta, \theta_p)$, less current is required to induce the same dynamic state at the same frequency. For the given angular dependence, this results in a compressed current interval for OPP oscillations in positive current and in an enlarged current interval for negative current, while keeping the frequency range constant (i.e., the upper frequency limit at $|J| = |J_{c2}|$ is the same for both current directions, see Ref. 14).

The oscillation frequency itself is dominated by the out-of-plane magnetization component M_z . Since M_z is proportional to the amplitude of the current density $|J|$ ⁹, this gives the approximate expression in Eq. (6) for the frequency

$$f \approx \frac{\gamma}{2\pi} 4\pi M_z \approx \frac{\gamma}{2\pi} \frac{g(\eta, \theta_p) J}{\alpha M_{st}}. \quad (6)$$

This relatively simple macrospin behavior of the frequency is more complex when the full micromagnetic configuration is taken into account via 3D micromagnetic modeling.

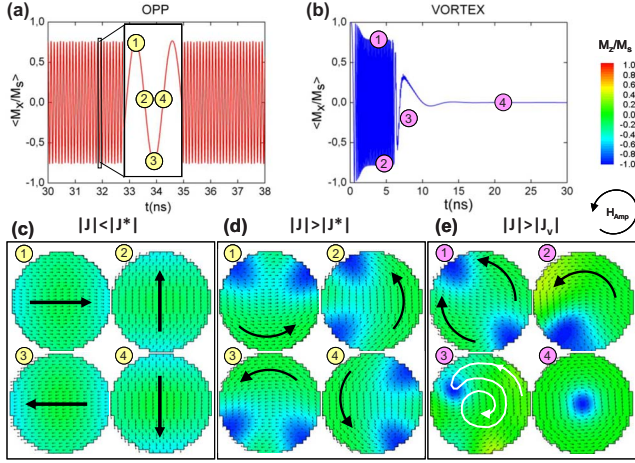


FIG. 4. (Color online) Time traces of the average M_x -component of the magnetization for (a) periodical OPP oscillations and (b) the transient to the static vortex state. Snapshots of the magnetization configurations (top view) at four different time intervals for a positive current density corresponding to (c) OPP oscillations on branch I, (d) OPP oscillations on branch II, and (e) the transition to a static vortex state. All simulations shown are performed for a circular disk of 60 nm diameter and including the Ampère field H_{Amp} . The color code to the right of (b) indicates the out-of-plane magnetization component. The schematics underneath indicates the rotation sense of the Ampère field for a positive current.

IV. MICROMAGNETIC SIMULATIONS

Due to the extensive computation time, we limit the discussion of the micromagnetic simulations to only the zero-field case $H_b=0$, upon increasing the amplitude of the current density J . Furthermore in this section, we consider only configuration [Fig. 1(a)] for a circular disk and neglect the Ampère field. Similar to the macrospin simulations, there is an IPS state at low amplitudes of the current density, where the FL magnetization is more or less uniform with a mean in-plane magnetization component that is aligned at an angle from the in-plane easy axis. However contrary to the macrospin simulations, the OPP and OPS states show a number of differences.

First of all, the amplitude of the critical current density $|J_{c1}|$ is slightly larger in the micromagnetic case than in the macrospin case. Second, in the OPP state for $|J| > |J_{c1}|$, the micromagnetic configuration changes abruptly at a current density labeled J^* in Fig. 3(a) (full dots). For low amplitudes of the current density $|J_{c1}| < |J| < |J^*|$ [called branch I in Fig. 3(a)], the magnetic configuration is quasiuniform with an S -like deformation and an overall small out-of-plane magnetization component [see Fig. 3(c)]. During one precession cycle, this configuration does not change and it rotates almost uniformly and coherently behaving approximately like a macrospin [see Fig. 4(c)].

Above a certain amplitude of the current density $|J| \geq |J^*|$, called branch II in Fig. 3(a), the magnetization configuration transits into an onion-type configuration shown in Fig. 3(c), with two “out-of-plane” domains of strong out-of-plane magnetization component where the in-plane magnetic moments meet head to head. At the transition current density

$|J^*|$, this onion state is symmetric and the two out-of-plane domains are 180° apart. Upon increasing the amplitude of the current density, a more and more pronounced C -like distortion of the onion state develops [see Fig. 3(c)], moving the two out-of-plane domains closer together. At the same time, the out-of-plane magnetization component in these domains increases. During one precession cycle this whole configuration rotates coherently without distortion, as shown in Fig. 4(d).

We note that despite some apparent similarity, the out-of-plane domains are not vortices since the in-plane magnetic moments do not curl as is typical for a vortex but meet head to head as in an onion state. Furthermore, the rotation sense of these domains is opposite to the one expected for a vortex whose vortex core would point into the same direction as the out-of-plane domains.²³ For example the configuration in Fig. 4(d) rotates counterclockwise, while a vortex would rotate clockwise. The rotation sense of the out-of-plane domains is determined by the macrospinlike oscillation of the surrounding in-plane spins, which “drag” the out-of-plane domain with it.

For a sufficiently large amplitude of the current density, $|J| > |J_v|$, the two out-of-plane domains are no longer stable. As revealed by the transient configurations as a function of time in Fig. 4(e), the out-of-plane domains first approach each other and then collapse to a single domain, giving rise to the formation of a vortex on the border of the circular disk. This vortex then moves on a spiral trajectory from the edge to the center of the disk. Consistent with what was mentioned above, the rotation sense of this spiral trajectory is opposite to the one of the out-of-plane domains. This is indicated by the white arrow in Fig. 4(e) (configuration 3). The motion of the vortex slows down a lot and finally the vortex stabilizes in the center of the circular disk [Figs. 3(c) and 4(e)].

Hence, it seems that the OPS state, which occurs in the macrospin approach for amplitudes of the current density $|J| > |J_{c2}|$, is replaced by a stable vortex state in the micromagnetic simulation when $|J| > |J_v|$. However, the OPS macrospin state, for which all magnetic moments align out of plane, can also be obtained in the micromagnetic approach for very large current densities (for example, in positive current for $J \approx 10J_v = 35 \cdot 10^{11}$ A/m²).

In the following, we concentrate only on the OPP configuration and in particular on the frequency versus current dependence given in Fig. 3(a) (full dots). From the macrospin approach, we have seen that the precession frequency is determined by the out-of-plane magnetization component M_z . This is essentially also the case for the micromagnetic configuration. As shown in Fig. 3(b), for branch I ($|J| < |J^*|$) the mean magnetization component $\langle M_z \rangle$ and therefore the frequency increases with current. Furthermore, the frequencies of branch I are almost the same as in the macrospin approach. This reflects the more or less coherent rotation of the almost uniform magnetization configuration of branch I as shown in Fig. 4(c).

At the transition from branch I to branch II ($J \sim J^*$) corresponding to the transition from the macrospinlike uniform configuration to the nonuniform configuration, an abrupt jump occurs in the mean $\langle M_z \rangle$ component accompanied by a

1 GHz jump in the frequency. This change in the configuration can qualitatively be explained by the competition between the demagnetizing field torque, which favors an in-plane orientation of the magnetization and the spin-transfer torque that pushes the magnetization out-of-plane, leading to a strong out-of-plane demagnetization field energy. Thus in order to reduce the demagnetization field energy at large values of the current, a good compromise is to develop areas of alternating out-of-plane magnetization components. This can be considered similar to the formation of stripe domains in perpendicular anisotropy materials.²⁴

As shown in Figs. 3 and 4, the out-of-plane magnetization is concentrated in the two domains where the in-plane magnetization meets head to head in the onion or *C*-like configuration. In contrast, in the rest of the circular disk the magnetic moments are pushed back into the film plane due to the additional dipolar field emanating from the out-of-plane domains. This leads to an overall reduction of the mean out-of-plane magnetization component $\langle M_z \rangle$ as a function of increasing current density [see Fig. 3(b)] and consequently to a saturation or reduction in the frequency when $|J| > |J^*|$.

V. AMPÈRE FIELD EFFECT

The above simulations have been obtained for configuration [Fig. 1(a)] in the absence of the Ampère field. The *C*-like distortion of the onion state can therefore not be attributed to an Ampère field effect. This is underlined by the fact that for the example in Fig. 3(c), the distortion is opposite to the one expected from the Ampère field. We suggest here that the *C*-like distortion is a further way to reduce the out-of-plane demagnetization field energy. By moving the two out-of-plane domains closer together the total volume of the area with strong out-of-plane magnetization is reduced.

Including the Ampère field, we see from the simulation that the *C*-like distortion appears almost immediately after the jump at J^* . However, since its maximum value at the outer diameter of the circular disk is much less than the out-of-plane demagnetization field, it does not influence the OPP oscillation frequency very much. As shown in Fig. 3(a) (open dot), the overall evolution of both branches I and II of the frequency vs current dispersion is the same. The current dependence of the average out-of-plane magnetization component in Fig. 3(b) (open dots) confirms this observation. The major effect of the Ampère field is at larger currents with a current interval of branch II that is extended to slightly larger values (negative and positive). This is somewhat counterintuitive but might suggest that the collapse of the two out-of-plane domains before the vortex formation of Fig. 4(e) is “delayed,” due to the Ampère field. Without further mentioning, in the rest of the presentation the Ampère field is included in the simulations.

VI. SCALING OF THE CURRENT AXIS

In conclusion of the above discussion, in the micromagnetic simulations there exist two branches of OPP oscillations, which are characterized by an abrupt change in the slope of the frequency vs current density at $J=J^*$. In the

experiments,¹⁵ a similar behavior has been obtained. In particular, two frequency branches with similar changes of their slopes were observed [see Fig. 6(a) below]. While this suggests that the experimental data can be qualitatively explained by the micromagnetic simulations described in Sec IV, differences exist in the current interval where these two branches occur as well as in the absolute values of the frequencies, which are about two to three times larger in the simulations than in the experiments [compare Fig. 6(a) below].

The difference in the current interval might be explained qualitatively as follows. As argued in Sec. III the current density is scaled by the spin-polarization efficiency $g(\eta, \theta_p)$. Its angular dependence produces an asymmetry of the f vs J dispersion with a steeper slope and reduced current interval in positive current as compared to negative current. The same asymmetry is observed in the micromagnetic simulations shown in Figs. 3(a) and 5(a) (open circles). For example, the transition from branch I to branch II occurs at a larger current value for negative current. However, the maximum frequency and the frequency at the transition J^* as well as their corresponding average $\langle M_z \rangle$ components are the same for positive and negative current [see Figs. 3(a) and 3(b)]. The spin-polarization efficiency thus remains a scaling factor for the current density in the micromagnetic approach for both branches I and II, changing only the current interval where the oscillations occur but not their frequencies.

In the same way we have checked that the damping constant represents a scaling of the current axis. This is demonstrated in Fig. 5(a), where for the circular disk the frequency vs current-density amplitude is shown for two values of the damping constant: $\alpha=0.01$ and $\alpha=0.02$. For stronger damping, a larger current-density amplitude is required in order to stabilize an OPP steady-state oscillation at a given frequency f . Thus the total current range where OPP oscillations exist is larger for larger α ; however, the maximum frequency and the frequency at J^* remain unchanged [see Fig. 5(a)].

The different current intervals observed in the experiment and the simulations for OPP oscillations might thus be attributed to the precise values of the damping parameter and the spin polarization, which are both not well known for the experimental studies. In contrast to this, the maximum frequency, which is unchanged by g and α , is by a factor of 2–3 larger in the simulations than in the experiments [compare Fig. 6(a)], indicating that there are other contributions. The above calculations made two major assumptions that do not represent the experimental configuration. First, the full nanopillar stack contains three magnetic layers as shown in Fig. 1(b). The inhomogeneous static dipolar interaction fields from the polarizing and the free layer can take considerable values (up to 160 kA/m or 2 kOe oriented mostly out-of-plane) at the position of the free layer, as shown in Fig. 1(b), and can influence the dynamic magnetization configuration. The second difference is the element shape which in the experiment is an ellipse of nominal size of 60×70 nm², while it is a circular disk in the simulations above. In Secs. VII and VIII, we therefore present independently the effect of the static dipolar interaction field for the circular element (using $\alpha=0.01$) and the influence of the elliptical shape (using $\alpha=0.02$).

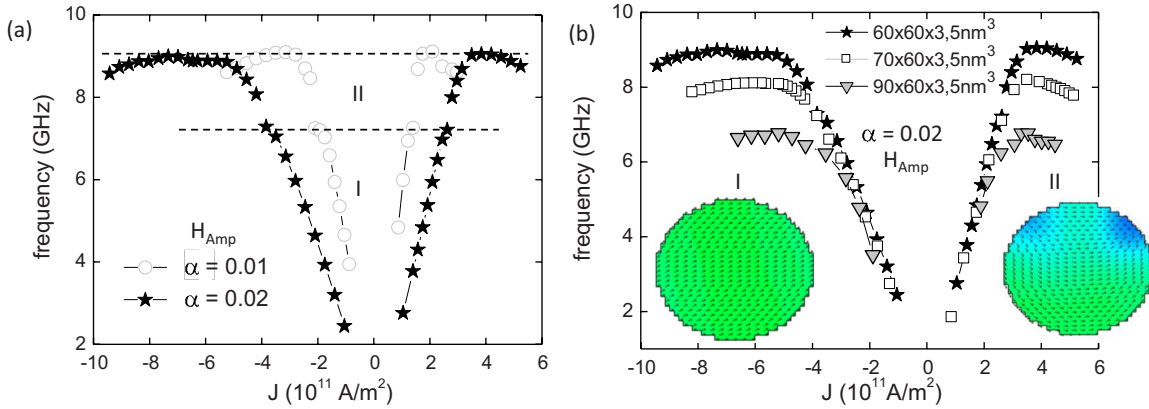


FIG. 5. (Color online) (a) Frequency vs current-density amplitude for two values of the damping constant with $\alpha=0.01$ [open dots, same as Fig. 3(a) open dots] and $\alpha=0.02$ (full stars). In both cases, the Ampère field has been taken into account. The horizontal dotted lines indicate that the maximum frequency value as well as the frequency value at J^* are independent of the value of α . (b) Frequency vs current-density amplitude using $\alpha=0.02$ and including the Ampère field for three sample shapes: circular disk of 60 nm diameter (full stars) and ellipses of $60 \times 70 \text{ nm}^2$ (open square) and $60 \times 90 \text{ nm}^2$ (full triangle). The insets show the magnetization configuration of the $60 \times 70 \text{ nm}^2$ ellipse on branch I (left) and branch II (right).

VII. INFLUENCE OF THE STATIC DIPOLAR INTERACTION FIELD

In Fig. 1(b) the spatial distribution of the three components of the static dipolar interaction field inside the free layer is shown under the assumption that the polarizer is uniformly magnetized along the $+Oz$ direction and the analyzer is uniformly magnetized along the $-Ox$ direction. This field displays an asymmetric “fanlike” distribution, with an out-of-plane component that is stronger at the right edge of the circular disk than at the left edge. The overall values of these dipolar fields are quite important.

Since the static dipolar interaction field emanating from the analyzer is mainly in plane, it can be described by an average in-plane field that leads to a shift of the hysteresis loop. Such a shift is also evident in the experiments.¹⁵ Therefore, as in the experiments, we have compensated the static dipolar interaction field from the analyzer by applying external fields of 46.75 mT (467.5 Oe) oriented into the negative direction of the Ox axis so that we study the behavior in zero effective external field. The field value has been estimated by calculating by micromagnetic simulations the shift of the hysteresis loop of the free layer.

Taking into account only the static dipolar interaction field of the analyzer in the simulations, we have obtained the same evolution of the micromagnetic configuration and of the frequency as a function of current, as the one shown in Figs. 3 and 4. There are almost no changes in the absolute values of the frequency for both branches of f vs J . The static dipolar interaction field from the analyzer has thus no major effect on the OPP dynamics and represents only a shift on the field axis.

On the contrary, when we include also the static dipolar interaction field from the polarizer, there are some important modifications of the magnetic configuration and the frequency. First of all, in zero current, the average out-of-plane magnetization is nonzero since the static dipolar interaction field from the polarizer pushes the magnetization out-of-plane into the positive z direction [see Fig. 6(b)]. This re-

duces the current value for the onset of the OPP oscillations (for increasing current). Second, due to the stray field from the analyzer, the out-of-plane magnetization component of the dipolar field is asymmetric in the Ox direction, being positive at the right edge and negative at the left edge [see Figs. 1(b) and 6(c)]. Third, in contrast to the onion state of Fig. 3(c), the in-plane magnetization component follows the

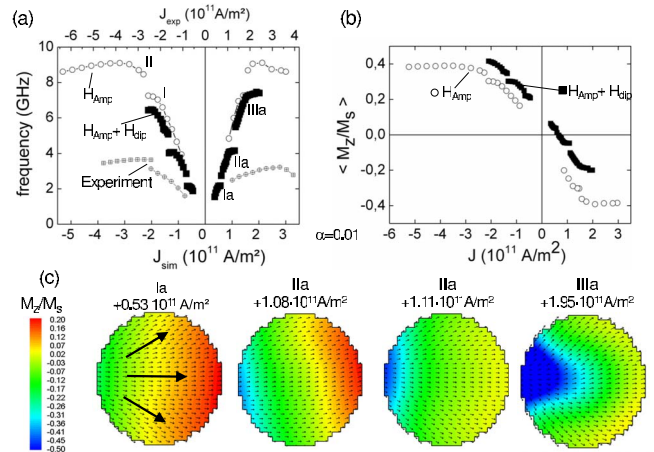


FIG. 6. (Color online) (a) Comparison of the f vs J dependence for simulations ($\alpha=0.01$) including the static dipolar interaction field (H_{dip}) from the polarizer and analyzer (full squares), simulations ($\alpha=0.01$) without static dipolar interaction field as in Fig. 3(a) (open dots), and the experiments (crossed dots and squares). In both simulations, the Ampère field H_{Amp} has been included. The three branches of the simulation including H_{dip} are denoted by Ia, IIa, and IIIa. The bottom current scale J_{sim} is for the simulation data; the top current scale J_{exp} is for the experimental data. (b) Mean value of $\langle M_z/M_s \rangle$ for the simulations without (open dots) and with (full squares) static dipolar interaction field and including the Ampère field. (c) Cross-sectional view of the magnetization distributions of the free layer for different positives values of J of the three branches Ia, IIa, and IIIa. The arrows for the configuration to the left indicate the fanlike spread of the magnetization.

total dipolar interaction field adopting a fanlike configuration [compare Figs. 1(b) and 6(c)].

The current evolution of this dynamic fanlike magnetization configuration is shown in Fig. 6(c) together with the frequency vs. current dependence in Fig. 6(a). We see that the transition into a static vortex state occurs at a current value, which is comparable to the current J^* for the zero dipolar field case. In consequence the maximum frequency is reduced by 20%–30%. Furthermore, the frequency seems overall to increase as a function of current and to be close to the values of branch I [Fig. 3(a)], while the saturation of the frequency [branch II of Fig. 3(a)] is absent. Finally, the increase in the frequency vs current is not continuous and contains two discrete jumps. This leads to the three branches denoted by Ia, IIa, and IIIa in Fig. 6(a) for the dipolar field case.

Although the saturation branch II [Fig. 3(a)] is absent, the dynamics of branch IIIa is similar to the one of branch II, the difference being that instead of two out-of-plane domains, only one out-of-plane domain exists, which is at the base of the fanlike configuration. This out-of-plane domain rotates around the circular disk, leading to a simultaneous rotation of the fanlike configuration during one precession period. This rotation is similar to the one shown in Fig. 4(d).

In contrast to the macrospinlike rotation of branch I of the zero dipolar field case, in the presence of the dipolar field, the out-of-plane domain is present for all current values [see Fig. 6(c)]. However it is less pronounced on branches Ia and IIa [see the M_z scale of Fig. 6(c)]. Furthermore, the jumps between the branches are not associated with an evident change in the magnetization configuration as in the zero dipolar case; thus their origin seems to be more subtle.

In conclusion, the overall current dependence contains a number of differences in the presence of the static dipolar interaction field, despite the resemblance of the frequency vs current curve of branches Ia, IIa, and IIIa to branch I in Fig. 6(a). These differences, in particular, the multiple jumps in the frequency, are not yet well understood and require much more detailed analysis. The importance of the presented simulations is that they show a reduction in the maximum frequency, which might provide a possible explanation for the reduced frequency values observed in the experiments¹⁵ [see Fig. 6(a), top current scale J_{exp}]. In particular, when comparing the experimental maximum frequency (3–4 GHz), one might suggest that the experimental modes correspond to branches Ia and IIa. However, it is also possible that the experimental modes correspond to branches IIa and IIIa, when taking shape effects into account. As discussed in the next section an elliptical shape leads also to a reduction in the frequency.

VIII. SHAPE EFFECT

In the following we consider the influence of the sample shape on the precession frequency of the OPP oscillations, without considering the static dipolar interaction field from the polarizer or the analyzer. For this, we will compare simulations performed for a circular element of 60 nm diameter with those performed for two ellipses of 60×70 and 60

$\times 90$ nm². This corresponds to ellipticities of 1, 1.17, and 1.5. We have carried out the simulations for a damping parameter of $\alpha=0.02$ since this is closer to what has been estimated in the experiment.¹⁵ Also, the OPP oscillations in the case of the ellipses have been obtained by starting with an OPS state and reducing the current to the given values. Finally, in the case of the ellipses the uniaxial anisotropy energy constant K_u was taken to be zero and only the shape anisotropy is considered.

The obtained current dependence of the magnetization configuration and the frequency for the ellipses is very similar to the one of the circular disks, with two frequency branches I and II [see Fig. 5(b)]. In particular, for all three sample shapes the frequencies of branch I are more or less the same. This can be explained by the fact that branch I is more or less a macrospinlike OPP oscillation of a uniform magnetization state. While the shape anisotropy increases with increasing ellipticity (112 Oe for the 60×70 nm² element and 168 Oe for the 60×90 nm² element), it has little effect on the precession frequency. This has also been confirmed by macrospin simulations upon including a corresponding uniaxial anisotropy.

The values for the current density J^* for the transition of branch I to branch II however decrease with increasing ellipticity leading to much lower frequencies on branch II. As explained in Sec. III, the transition from branch I to branch II is due to a change of the magnetization configuration, which tends to reduce the out-of-plane demagnetization field energy. Assuming that this transition occurs at the same critical value of the total demagnetization field energy, then the square of the M_z component at the respective current densities J^* should scale inversely with the surface area. This is indeed verified from the simulations, which give a ratio of the square of the out-of-plane magnetization component M_z^2 at J^* of 1:1.07:1.3, which is close to the ratio of the ellipse surfaces (or equivalently to the ellipticity). Thus, upon increasing surface area, the corresponding M_z at J^* is lower explaining the decrease in frequency with increasing ellipticity.

IX. SUMMARY AND CONCLUSIONS

In summary, we have investigated via micromagnetic simulations the OPP precessions of a spin torque oscillator that is composed of a perpendicular polarizer and a planar free layer. The dependence of the frequency on the current density shows differences to the macrospin simulations^{9,13–15} for which the oscillation frequency increases continuously as a function of current density. In contrast to this, in the micromagnetic approach for circular disks, two f vs J branches exist. The low-current branch I corresponds to the coherent rotation of a macrospinlike uniform magnetization state, where the individual spins oscillate in phase on an OPP trajectory. The high-current branch II corresponds to the coherent rotation of a nonuniform magnetization state that contains two out-of-plane magnetized domains. These domains reduce the demagnetization field energy and rotate along the disk periphery on a circular trajectory. The corresponding frequency saturates or decreases with increasing current. For

still larger currents, a static vortex configuration replaces the macrospin OPS configuration.

It is emphasized that despite the nonhomogeneous magnetization configuration of branch II, the oscillation of the magnetization remains coherent. Furthermore the nonuniform dynamic magnetization state as well as the static vortex state are stable only in the presence of the spin torque. The nonuniform dynamic state is triggered by the demagnetization field energy, in a similar way as is the static stripe domain formation in perpendicular anisotropy materials²⁴ or the static vortex state in circular disks.²⁵ One might therefore state more generally that among the different effects of the spin torque, it is not only possible to rotate the magnetization into directions that are not energy minima (such as IPS or OPS) but that it can also induce new static or dynamic magnetization configurations, which are not stable in the absence of the spin polarized current.

The existence of the two current branches and the corresponding frequency range is not altered when including the Ampère field or increasing the damping parameter. The only effect is to change the current range for which the oscillations exist. However, when changing the shape of the element from circular to elliptical, the frequency of the second branch is much reduced. Finally, when taking also the static dipolar interaction fields into account, the dynamic magnetization configuration is considerably changed. First the uniform or onionlike configuration is replaced by a fanlike configuration. Second, instead of two, only one out-of-plane

domain exists, which is present almost in the whole current range and that most likely facilitates the transition into the vortex state. As a consequence, the current and frequency range are much reduced. Furthermore multiple jumps occur in the f vs J dependency, which are not associated with an evident change of the magnetization configuration.

When comparing the simulations to recent experiments,¹⁵ the two experimentally observed branches can be qualitatively explained, corresponding to the transition from a homogenous to an inhomogeneous magnetization configuration. The different ranges of current where these two branches are observed depend on the spin-polarization factor and the damping constant. Finally, the simulations suggest that the reduced experimental frequencies might be due to a combined effect of the elliptical shape and static dipolar interaction fields.

ACKNOWLEDGMENTS

This work has been supported in part by the French National Program ANVAR Grant No. A0503013 and by the French National Agency (ANR) through the programs CARNOT and PNANO (MagICO Grant No. ANR-05-NANO-044), as well as partially by the EC Program DYNAMICS Grant No HPRN-CT-2002-00289. I.F. acknowledges support from the CARNOT program. We thank A. Slavin, V. Tiberkevich, and C. Baraduc for very stimulating discussions.

¹J. C. Slonczewski, U.S. Patent No. US5695864 (1997).

²J. C. Slonczewski, *J. Magn. Magn. Mater.* **159**, L1 (1996).

³L. Berger, *Phys. Rev. B* **54**, 9353 (1996).

⁴S. I. Kiselev, J. C. Sankey, I. N. Krivorotov, N. C. Emley, R. J. Schoelkopf, R. A. Buhrman, and D. C. Ralph, *Nature* (London) **425**, 380 (2003).

⁵S. I. Kiselev, J. C. Sankey, I. N. Krivorotov, N. C. Emley, M. Rinkoski, C. Perez, R. A. Buhrman, and D. C. Ralph, *Phys. Rev. Lett.* **93**, 036601 (2004).

⁶W. H. Rippard, M. R. Pufall, S. Kaka, T. J. Silva, and S. E. Russek, *Phys. Rev. B* **70**, 100406(R) (2004).

⁷W. H. Rippard, M. R. Pufall, S. Kaka, S. E. Russek, and T. J. Silva, *Phys. Rev. Lett.* **92**, 027201 (2004).

⁸Q. Mistral, J. V. Kim, T. Devolder, P. Crozat, C. Chappert, J. A. Katine, M. J. Carey, and K. Ito, *Appl. Phys. Lett.* **88**, 192507 (2006).

⁹K. J. Lee, O. Redon, and B. Dieny, *Appl. Phys. Lett.* **86**, 022505 (2005).

¹⁰A. D. Kent, B. Özyilmaz, and E. del Barco, *Appl. Phys. Lett.* **84**, 3897 (2004).

¹¹H. Morise and S. Nakamura, *Phys. Rev. B* **71**, 014439 (2005).

¹²W. Jin, Y. Liu, and H. Chen, *IEEE Trans. Magn.* **42**, 2682 (2006).

¹³I. Firastrau, U. Ebels, L. D. Buda-Prejbeanu, J. C. Toussaint, C. Thirion, and B. Dieny, *J. Magn. Magn. Mater.* **310**, 2029 (2007).

¹⁴U. Ebels, D. Houssameddine, I. Firastrau, D. Gusakova, C. Thirion, B. Dieny, and L. D. Buda-Prejbeanu, preceding paper, *Phys. Rev. B* **78**, 024436 (2008).

¹⁵D. Houssameddine, U. Ebels, B. Delaët, B. Rodmacq, I. Firastrau, F. Ponthenier, M. Brunet, C. Thirion, J.-P. Michel, L. D. Buda-Prejbeanu, M.-C. Cyrille, O. Redon, and B. Dieny, *Nat. Mater.* **6**, 447 (2007).

¹⁶L. D. Landau and E. Lifshitz, *Phys. Z. Sowjetunion* **8**, 153 (1935).

¹⁷W. F. Brown, Jr., *Micromagnetics* (Wiley, New York, 1963).

¹⁸J. Ch. Toussaint, B. Kevorkian, O. Fruchart, and J. Voiron, Proceedings of the Tenth International Symposium Magnetic Anisotropy and Coercivity in Rare-Earth Transition Metal Alloys, Dresden, Germany, 1998 (unpublished), p. 1001.

¹⁹D. Gusakova, I. Firastrau, A. Vedayev, D. Houssameddine, U. Ebels, J.-Ch. Toussaint, B. Dieny, and L. Buda-Prejbeanu, presentation SC15 of the 1st International Symposium on Advanced Magnetic Materials (ISAMMA2007), Jeju, Korea, 28 May–1 June 2007.

²⁰Z. Li and S. Zhang, *Phys. Rev. B* **68**, 024404 (2003).

²¹A. N. Slavin and V. S. Tiberkevich, *Phys. Rev. B* **72**, 094428 (2005).

²²M. D. Stiles and J. Miltat, in *Spin Dynamics in Confined Magnetic Structures III*, edited by B. Hillebrands and A. Thiaville (Springer, New York, 2006).

²³K. Yamada, S. Kasai, Y. Nakatani, K. Kobayashi, H. Kohno, A. Thiaville, and T. Ono, *Nat. Mater.* **6**, 289 (2007).

²⁴U. Ebels, L. Buda, K. Ounadjela, and P. E. Wigen, *Phys. Rev. B* **63**, 174437 (2001); A. Hubert and R. Schäfer, *Magnetic Domains* (Springer, New York, 1998).

²⁵L. D. Buda, I. L. Prejbeanu, U. Ebels, and K. Ounadjela, *Comput. Mater. Sci.* **24**, 181 (2002).